Crystal Structures of Human GAR Tfase at Low and High pH and with Substrate β-GAR[†,‡]

Yan Zhang,[§] Joel Desharnais,[§] Samantha E. Greasley,[§,||] G. Peter Beardsley,[⊥] Dale L. Boger,[§] and Ian A. Wilson*[,§]

Departments of Molecular Biology and Chemistry and The Skaggs Institute for Chemical Biology, The Scripps Research Institute, 10550 North Torrey Pines Road, La Jolla, California 92037, Departments of Pediatrics and Pharmacology, Yale University School of Medicine, 3094 LMP, 333 Cedar Street, P.O. Box 208064, New Haven, Connecticut 06520-8064

Received August 7, 2002; Revised Manuscript Received September 25, 2002

ABSTRACT: Glycinamide ribonucleotide transformylase (GAR Tfase) is a key folate-dependent enzyme in the de novo purine biosynthesis pathway and, as such, has been the target for antitumor drug design. Here, we describe the crystal structures of the human GAR Tfase (purN) component of the human trifunctional protein (purD−purM−purN) at various pH values and in complex with its substrate. Human GAR Tfase exhibits pH-dependent enzyme activity with its maximum around pH 7.5−8. Comparison of unliganded human GAR Tfase structures at pH 4.2 and pH 8.5 reveals conformational differences in the substrate binding loop, which at pH 4.2 occupies the binding cleft and prohibits substrate binding, while at pH 8.5 is permissive for substrate binding. The crystal structure of GAR Tfase with its natural substrate, β-glycinamide ribonucleotide (β-GAR), at pH 8.5 confirms this conformational isomerism. Surprisingly, several important structural differences are found between human GAR Tfase and previously reported *E. coli* GAR Tfase structures, which have been used as the primary template for drug design studies. While the *E. coli* structure gave valuable insights into the active site and formyl transfer mechanism, differences in structure and inhibition between the bacterial and mammalian enzymes suggest that the human GAR Tfase structure is now the appropriate template for the design of anti-cancer agents.

Glycinamide ribonucleotide transformylase (GAR Tfase)[1] catalyzes the first of two formyl transfer reactions in the de novo biosynthetic pathway of purines and, thus, is an enzyme of fundamental significance to the anabolism of all organisms (*1*−*3*). The conversion of glycinamide ribonucleotide to formyl glycinamide ribonucleotide uses 10-formyl-tetrahydrofolate (10-formyl-THF) as a cofactor in the pathway that leads to inosine monophosphate (IMP) and eventually to other purines (*1*).

The design of small-molecule antagonists of folic acid, acting on a number of critical folate-binding enzymes, such as dihydrofolate reductase (DHFR) (*4*, *5*), thymidylate synthetase (TS) (*6*, *7*), GAR Tfase, and 5-aminoimidazole-4-carboxamide-ribonucleotide transformylase (AICAR Tfase), has been an active area of drug discovery research for over 50 years (reviewed in refs *8* and *9*). Validation of GAR Tfase as a viable anticancer target came in the mid-1980s with the discovery of the first potent and selective inhibitor, 5,10-dideaza-5,6,7,8,-tetrahydrofolate (DDATHF) (*10*). The C-6 *R* isomer of DDATHF, referred to as lometrexol, entered clinical trials and demonstrated antitumor activity against a wide range of solid tumors (*11*).

Naturally occurring folate within mammalian cells is converted to a polyglutamated form by the addition of glutamate residues via a γ-peptide linkage by the action of folylpolyglutamate synthetase (FPGS) (*12*−*14*). Polyglutamation can increase the affinity of the folate-derivatives to GAR Tfase (*15*), as well as increase the overall negative charge on the folate molecule by 1 unit for each additional glutamate. The increased negative charges afforded by polyglutamation prevent transport of the folate derivatives back across the cell membrane and, therefore, enable retention within the cell. Folate analogues that use the folate binding protein and folate transporter are taken up into the cell. Polyglutamation then results in their sequestration within the cell and, hence, increases their cytotoxic potential (*16*, *17*).

Escherichia coli GAR Tfase is a monofunctional monomer of molecular weight of 23kDa but dimerizes below pH 6.8 (*18*). Investigation of the genetics of de novo purine biosynthesis in Drosophila and mammalian systems revealed that three enzymic activities, namely, GAR synthetase (purD), AIR synthetase (purM), and GAR Tfase (purN), are encoded by the same genetic locus, suggesting that all three activities reside on a single polypeptide chain (*19*−*21*). The

[†] This work was supported by the National Institutes of Health Grant PO1 CA63536 (I.A.W., D.L.B, and G.P.B.) and a Skaggs predoctoral fellowship (Y.Z.).

[‡] The coordinates for the human GAR Tfase at pH 8.5, pH 4.2, and in complex with substrate β-GAR structures have been deposited in the Protein Data Bank under file names 1MEJ, 1MEO, and 1MEN.

* Corresponding author. Phone: 858.784.9706. Fax: 858.784.2980. E-mail: wilson@scripps.edu.

[§] The Scripps Research Institute.

[||] Current address: Pfizer, La Jolla, 10770 Science Center Drive, San Diego, CA 92121.

[⊥] Yale University School of Medicine.

[1] Abbreviations: GAR Tfase, glycinamide ribonucleotide transformylase; β-GAR, β-glycinamide ribonucleotide; IMP, inosine monophosphate; DHFR, dihydrofolate reductase; TS, thymidylate synthetase; AICAR Tfase, 5-aminoimidazole-4-carboxamide-ribonucleotide transformylase; DDATHF, 5,10-dideaza-5,6,7,8-tetrahydrofolate; FPGS, folylpolyglutamate synthetase; 10-formyl-DDACTHF, 10-formyl-5,-10-dideaza-acyclic-5,6,7,8-tetrahydrofolic acid; 10-formyl-TDAF, 10-formyl-5,8,10-trideazafolic acid; 10-formyl-THF, 10-formyl-tetrahydrofolate; NCS, noncrystallographic symmetry.

10.1021/bi020522m CCC: $22.00
Published on Web 11/06/2002

GAR Tfase activity resides at the C-terminus of the trifunctional protein (purD−purM−purN) in eukaryotes. Human GAR Tfase domain has only 31% sequence identity to the *E. coli* protein; however, all of the key active site residues are conserved throughout the various known sequences from different species. The *E. coli* enzyme's lack of structural complexity, but close mechanistic similarity to the human trifunctional protein, made it an attractive candidate for previous studies of the biological role of this enzyme in purine biosynthesis and for the design of novel inhibitors for antineoplastic intervention. Extensive kinetic and structural studies have since then used *E. coli* GAR Tfase as the template for mechanistic studies (*3*, *22*−*24*) and for drug design (*25*−*28*), although some limited design on the human enzyme has also been reported (*29*).

However, even subtle differences within and around the protein active site might compromise the effectiveness of drugs targeted to the human enzyme, but designed against the *E. coli* enzyme template. For GAR Tfase, this concern surfaced when an aldehyde-based folate-analogue inhibitor 10-formyl-5,10-dideaza-acyclic-5,6,7,8-tetrahydrofolic acid (10-formyl-DDACTHF) was found to be more than 400 times more active against human GAR Tfase ($K_i = 14$ nM) than the *E. coli* enzyme ($K_i = 6\ \mu$M) (*28*). Furthermore, antifolates show totally different glutamation profiles toward the human versus the *E. coli* enzyme (*30*, *31*). These combined results suggest that a human GAR Tfase structure would provide a significantly better template for antitumor drug design than its bacterial counterpart.

E. coli GAR Tfase exhibits a pH-dependent activity profile with the maximum occurring between pH 8.0 and 8.5 with a nearly bell-shaped profile that drops at extreme pHs (*32*, *33*). *E. coli* GAR Tfase also shows a pH-dependent monomer−dimer equilibrium in solution, with the monomer preferably populated above pH 7.4 and the dimer below pH 6.6 (*18*). These solution studies are consistent with crystallization studies of GAR Tfase at various pH values. Wild-type, phosphate-bound GAR Tfase, crystallized at pH 6.75 (*34*, *35*), and the multisubstrate adduct complexed of *E. coli* GAR Tfase at pH 6.3 (*36*) are both dimeric, whereas the ternary enzyme complex with substrate β-GAR and 10-formyl-5,8,10-trideazafolic acid (10-formyl-TDAF) at pH 7.5 is monomeric (*25*) and an epoxide-derived multisubstrate adduct inhibitor complex with *E. coli* GAR Tfase at pH 7.4 (*26*) crystallize with four independent monomers in the asymmetric unit.

The proposal of a monomer−dimer transition near physiological pH as a control for the enzyme activity was an intriguing early speculation from these observations (*18*). To test this notion, a single-point mutant, Glu70Ala (E70A), of *E. coli* GAR Tfase was produced that disrupted dimerization even at low pH (*37*). Crystallization studies, as well as dynamic light scattering experiments and size exclusion chromatography, confirmed that the *E. coli* E70A mutant is monomeric at both low and high pH but, more importantly, had a kinetic pH-rate profile nearly identical to that of the wild-type enzyme (*33*). Thus, dimerization of *E. coli* GAR Tfase cannot then account for the observed decrease in enzyme activity at more acidic pH. Comparison of the high-resolution crystal structures of *E. coli* E70A GAR Tfase mutant at low and high pH (*33*) showed that a loop containing residues 111−131 is disordered at pH 3.5 but is well ordered above pH 7.5. This pH-dependent loop is in close proximity to the substrate-cofactor binding cleft. It was suggested that the loop could function as a hydrophobic lid to cover the active site (*33*), although its sequence is not totally conserved (45% identity) in the GAR Tfase domain of the human trifunctional protein.

Here, we show that the activity of human GAR Tfase is also pH-dependent. However, we propose that this pH-dependent activity in human GAR Tfase is due to its inability to bind the substrate, β-GAR, at low pH on the basis of our structural studies at high and low pH.

MATERIAL AND METHODS

Materials. The original plasmid of human GAR Tfase (cloneI) from the Beardsley lab was used to initiate the human GAR Tfase (purN) studies. The primer used to clone new constructs was synthesized by Retrogen, La Jolla, CA. The cofactor, 10-formyl-THF, was synthesized as described previously (*38*). Due to the relative instability of the cofactor, the pH-dependent activity assay was completed within 24 h after the compound was synthesized. The substrate, (α,β)-GAR, was synthesized as described previously (*39*). Luria broth (LB) and agar were obtained from Life Technologies, Gaithersburg, MD. All common buffers and reagents were purchased from Sigma-Aldrich Corp., St. Louis, MO.

Protein Cloning and Expression. The cloneI containing the GAR Tfase domain (residues 810−1010 of the trifunctional protein) was originally subcloned into a pet23d vector at a BsmI/XhoI site with a C-terminal hexahistidine tag to facilitate the production and purification of the protein. We also designed a second clone (cloneII) starting at an earlier site (residue 808) that was cloned into a pet22b vector using an NdeI/XhoI site. For both clones, BL21 (DE3) Gold cells were used to achieve stable expression and high yields of protein. For the cloneI, the bacterial culture grew to an absorbance of 0.6 at 595 nm from a freshly streaked plate at 37 °C, which was then induced with 0.1 mM IPTG at 20 °C for 9 h. This low concentration of IPTG and temperature substantially improved the protein solubility. The cloneII was induced with 0.5 mM IPTG at room temperature for 5 h after its absorbance reached 0.8.

Protein Purification. The cells for the two clones were disrupted by sonication in a buffer of 0.5 M NaCl, 50 mM Hepes, pH 7.9, 10% glycerol, 0.1% Triton, and the lysate was clarified by centrifugation at 20 000*g* for 50 min. The supernatant was then incubated with 10 mL of nickel affinity beads (Qiagen Inc., Valencia, CA) for 3 h. The beads were washed extensively with 0.5 M NaCl, 10mM Imidazole, 25 mM Hepes, pH 7.9, until the baseline for the absorbance became flat. The protein was eluted with a 10−250 mM Imidazole gradient. Fractions containing protein were detected by SDS−PAGE and pooled. For cloneI, the major contamination, as assessed by SDS−PAGE and mass spectrometry, was a 66kDa polypeptide which was then removed by gel filtration on a superdex75 (Amersham Pharmacia Biotech, Piscataway, NJ) column, equilibrated with 0.2 M NaCl, 25 mM Tris, pH 8.0, 10 mM β-mercaptoethanol. The cloneII protein after elution from a nickel column was further purified by a second application of nickel affinity chromatography. The purity of both proteins was assessed by SDS−PAGE and indicated higher than 99% purity. Both proteins

Table 1: Data Collection and Refinement Statistics for Phosphate-Bound and Substrate-Bound Human GAR Tfase at pH 8.5 and pH 4.2

	unliganded at pH 8.5	substrate-bound at pH 8.5	unliganded at pH 4.2
	Data Collection		
space group	*R*32	*R*32	$P6_522$
no. molecules per asu	3	3	1
resolution (Å)	30−2.0 (2.10−2.0)[a]	43−2.23 (2.30−2.23)	46−1.72 (1.78−1.72)
# observations	118898	144600	167456
# unique reflections	53638	38266	40379
multiplicity	2.21	3.78	4.15
completeness (%)	97.8 (96.8)	98.5 (86.4)	98.7 (99.0)
R_{sym}[b] (%)	6 (37.2)	7.6 (51.0)	7.2 (41.8)
I/σ	11.2 (1.6)	24.3 (2.5)	23.4 (1.6)
	Refinement		
R_{cryst}[c] (%)	21.4	22.0	22.5
R_{free}[d] (%)	25.2	26.7	24.0
number of protein atoms	4557	4557	1532
number of waters	448	128	148
average *B*-value (Å^2)	29.9	44.1	25.3
average solvent *B*-value (Å^2)	34.1	37.9	34.4
average ligand *B*-value (Å^2)	−	41.2	−
rms deviations from ideal			
bond lengths (Å)	0.0085	0.0084	0.0080
bond angles (deg)	1.34	1.45	1.14
Ramachandran plot (%)			
most favored	90.8	91.2	92.6
additionally allowed	9.2	8.8	7.4

[a] Numbers in parentheses refer to the highest resolution shell. [b] $R_{merge} = [\sum_h\sum_i|I_i(h) - \langle I(h)\rangle > |/\sum_h\sum_i I_i(h)] \times 100$, where $\langle I(h)\rangle$ is the mean of the $I(h)$ observation of reflection. [c] $R_{cryst} = \sum_h||F_o| - |F_c||/\sum_h|F_o|$, where F_o can F_c are the observed and calculated structure factor amplitudes.[d] R_{free} (%) is the same as R_{cryst}, but for 10% of the data randomly omitted from refinement.

show a single band with a pI ∼6.5 on isoelectric focusing gels. Each liter of cloneI broth can produce 8 mg of pure protein, while 40 mg of pure protein can be obtained per liter of cloneII broth. Both protein clones were used in our kinetic activity assays and crystallization experiments.

Kinetic Activity Assay. The same pH buffer was used in the pH-dependent activity assay containing 50 mM acetate, 50 mM bis-propane, 50 mM CHES, and 150 mM NaCl. The buffer was adjusted to the following values with HCl or NaOH: 4.2, 5.5, 6.1, 6.5, 6.9, 7.2, 7.4, 7.8, 8.1, 8.5, 8.8, 9.1, 9.5, and 9.8. The substrate, β-GAR, at 0.2 mM concentration was mixed with the buffered protein solution and the reaction initiated by the addition of 20 μM of cofactor. The reaction was performed in a Spectra Max 250 (Molecular Devices Inc, Sunnyvale, CA), similar to a previously described method (*40*). The data were fitted to eq 1 (*41*) using KaleidaGraph (Abelbeck Software, Version 3.0.5):

$$K_{cat}(\mathrm{pH}) = K_{max}(1 + 10^{\mathrm{p}K_{a1}-\mathrm{pH}} + 10^{\mathrm{pH}-\mathrm{p}K_{a2}})^{-1} \quad (1)$$

Crystallization and Data Collection. The proteins of both clones were screened for initial crystallization conditions by the method of vapor diffusion in sitting drops (*42*). The protein solution was mixed with an equal volume (2 μL) of precipitating solution and left to equilibrate at 4 °C. The cloneI protein crystallized at a concentration of 10 mg/mL from 18−21% PEG4K, 2% PEG400, 0.1 M NaCl, 0.1 M Tris, pH 8.5. A plate-shaped crystal (0.6 mm × 0.4 mm × 0.05 mm) was obtained after 6 days. Data were collected on a MAR345 Research imaging plate at beam line 9-1 of the Stanford Synchrotron Radiation Laboratory (SSRL) at −178 °C by flash-cooling a crystal cryoprotected with 12% PEG400 in the nitrogen gas stream. The substrate soaking experiment was performed on a crystal at pH 8.5 soaked overnight in mother liquor with 2 mM (α,β)-GAR. Data for the complex were collected on a MAR Research imaging plate on beam line 5.0.2 at Berkeley Advanced Light Source (ALS). Both data sets were processed and scaled with HKL2000 (*43*). The unliganded and substrate complex crystals at pH 8.5 belong to space group *R*32, with unit cell dimensions a = *b* = 152.5 Å, *c* = 193.4 Å, γ = 120° and a = *b* = 147.8 Å, *c* = 189.5 Å, γ = 120°, respectively. There are three molecules per asymmetric unit based on the estimated Matthews coefficient (*44*) of 3 and 2.8 Å^3 Da^{-1} for free and bound enzyme. Data statistics for each data set are given in Table 1.

The low-pH crystals grew from cloneII protein at 20 mg/mL in 1.9−2.1 M ammonium sulfate, 0.1 M acetate buffer, pH 4.2−4.6. To try to obtain the substrate-bound complex at low pH, crystals were either soaked in 4 mM (α,β)-GAR overnight or from cocrystallization experiments with 0.5 mM substrate. Glycerol at 25% was used as cryo-protectant. Data were collected on an ADSC 3 × 3 CCD detector at beamline 11-1 at SSRL. All three sets of crystals (unliganded, attempted soak and cocrystallized with substrate at pH 4.2) belong to space group of $P6_522$ with one molecule per asymmetric unit. The Matthews coefficient (*44*) for this crystal form ranges from 4.4 to 4.6, which translates to a relatively high solvent content of ∼75%. The soaked and cocrystallized data sets have R_{sym} values of 5.5% and 6.2% and completeness of 99.7% and 96%, respectively. Only the data collection statistics for the unliganded human GAR Tfase at pH 4.2 are reported in Table 1, as β-GAR could not be found in any of the electron density maps calculated from low pH data.

Structure Solution and Refinement. The structure of unliganded human GAR Tfase at pH 8.5 (high pH model:

hgar) was determined by molecular replacement (MR) (*45*) using the *E. coli* GAR Tfase in complex with β-GAR and 10-formyl-TDAF (PDB code 1C2T) (*25*) as the search model in Molrep (CCP4 program suite) (*46*). All of the nonconserved amino acids were truncated to alanine; waters and substrate/cofactors were excluded from the search model. Once refined, this model became the search model for the substrate-bound human GAR Tfase complex at pH 8.5, unliganded human GAR Tfase at pH 4.2 (low pH model: lgar) and the attempted soaked and cocrystallized crystals for human GAR Tfase at low pH. Molrep (*46*) was used to find the solution for substrate-bound protein complex at pH 8.5. The low-pH crystal structures were determined by Molecular Replacement with AmoRe (*47*).

Refinement for all of the models was carried out using the program CNS (*48*). The CNS program package allows rigid-body refinement, energy-restrained minimization protocols, and simulated annealing procedures for refinement. The structures were refined by means of iterative cycles of torsion angle dynamics using a maximum likelihood target function and either slow cooling or constant temperature protocols (*49*) in CNS. A bulk solvent correction with a flat model and anisotropic temperature value correction was used throughout the refinement. Model building was performed in O (*50*) using a combination of shake-omit 2Fo−Fc and Fo−Fc density maps. A test set of 10% of reflections was omitted from each data set for the calculation of R_{free} (*51*).

Since unliganded and substrate-bound human GAR Tfase crystals at pH 8.5 contain three molecules per asymmetric unit, the calculated phases were improved by 3-fold noncrystallographic symmetry (NCS) averaging in combination with solvent flattening and histogram matching with DM (*52*). NCS restraints were released for the more disordered regions of the structure (residues 21−26, 58−63, 141−145, and 190−200). During the last round of refinement, all NCS restraints were released, resulting in a final R_{cryst} and R_{free} of 21.4% and 25.2% for unliganded GAR Tfase at pH 8.5 and 22.0% and 26.7% for substrate-bound complex at pH 8.5.

For human GAR Tfase at pH 4.2, the final refinement was implemented in the CCP4 program TLS refinement (*53*). The final R_{cryst} and R_{free} are 22.5% and 24.0%, respectively. The crystals soaked and cocrystallized with substrate at low pH also refined to reasonable R_{free} values (23.6% and 23.4%, respectively), but, as indicated previously, no electron density corresponding to the substrate was observed.

Structure validation was carried out with Procheck (*54*). All models show excellent stereochemical quality, with more than 90% of the residues in the most favored regions of the Ramachandran plot with no outliers. The final statistics for the crystal structures of human GAR Tfase at pH 8.5 and pH 4.2 are summarized in Table 1.

RESULTS AND DISCUSSION

Enzyme Activity Profile. Due to the complexity of the human trifunctional protein and our special interest in GAR Tfase, the expression constructs contained only the human GAR Tfase domain (purN). The individual GAR Tfase domain of human trifunctional enzyme retains comparable enzymatic properties to those of the native trifunctional protein (*55, 56*). Furthermore, the marked kinetic similarities between recombinant human GAR Tfase domain and its corresponding activity in the trifunctional enzyme suggest that the GAR synthetase and GAR Tfase activities of the trifunctional enzyme act independently (*40*), although substrate sequestration may be facilitated within the trifunctional complex.

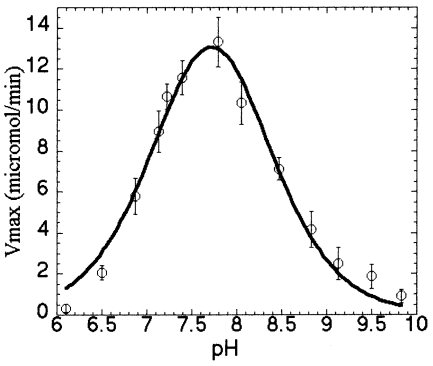

FIGURE 1: Human GAR Tfase activity vs pH. The *X*-axis represents pH, and the *Y* axis represents V_{max} under assay conditions. The results shown are the average of three measurements for each condition. Data curves are fitted with KaleidaGraph (Abelbeck Software, Version 3.0.5) fitted in eq 1.

For *E. coli* GAR Tfase, the enzyme has a pH-dependent activity with its maximum observed between pH 8−8.5. Several hypotheses have been proposed for this pH dependence. One is the loss of activity due to dimerization, but this idea was dismissed when the engineered mutant E70A, which is an obligate monomer, displayed a wild-type pH-activity profile. Another proposal from our own work (*33*) showed an order−disorder transition of the loop 111−131, which is ordered only at high pH in the electron density maps. To test whether this pH dependence is conserved in the human enzyme, the human GAR Tfase recombinant protein was similarly tested for its activity at various pHs. The same buffer (50 mM acetate, 50 mM bis-propane, 50 mM CHES, and 150 mM NaCl) was used throughout the assay to minimize buffer interference. The protein was oversaturated with both substrate (0.25 mM) and cofactor (20 μM), based on the published K_m for substrate (0.94 $\pm$ 0.21 μM) and cofactor (1.58 $\pm$ 0.25 μM) (*56*). The specific activity of the recombinant human GAR Tfase is consistent with previous results under similar conditions (V_{max} = 13.3 $\pm$ 1.2 μmol/min vs 17.4 $\pm$ 1.4 μmol/min, as reported for recombinant human GAR Tfase domain, ref *40*). The human protein also shows a bell-shaped activity profile, with a maximum activity around pH 7.5−8.0 (Figure 1). Enzyme activity is lost rapidly on reduction of pH, with no activity observed below pH 6 under the assay conditions (Figure 1). Therefore, under crystallization conditions at pH 4.2, the protein has negligible activity. However, at pH 8.5, the GAR Tfase retains more than half of its maximum activity. Thus, at pH 8.5, GAR Tfase is in its active form, whereas at pH 4.2, it corresponds to an inactive protein.

Overall Structure. The structures described herein include unliganded human GAR Tfase at pH 8.5 (hgar) human GAR Tfase in complex with substrate, β-GAR, at pH 8.5, both from construct cloneI, and unliganded human GAR Tfase at pH 4.2 (lgar) from construct cloneII. The sequence differences of the two clones are only the first two residues Ala and Arg at the N-terminus, which are not involved in the formyl transfer reaction. Although the crystals were processed and refined independently, the soaked and coc-

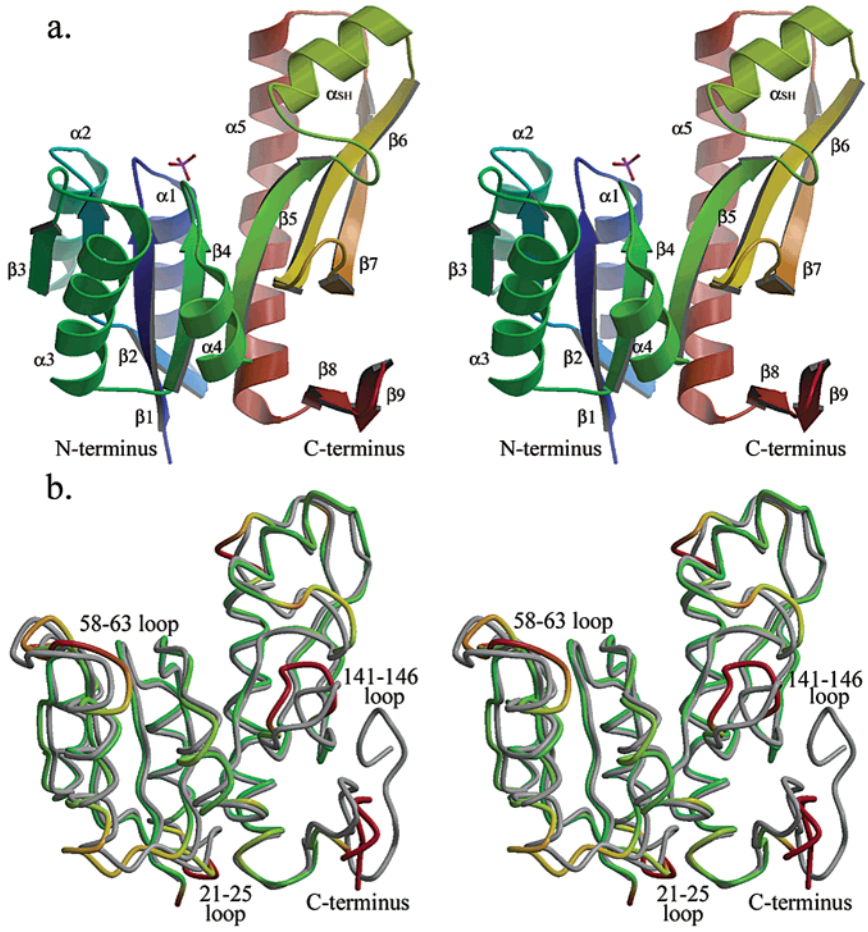

FIGURE 2: Human GAR Tfase structure. (a) Stereo ribbon diagram of the overall topology of unliganded human GAR Tfase at pH 8.5 (hgar). Helices are shown as coils and β-strands as extended arrows and labeled according to the *E. coli* GAR Tfase structure (*34*). α_{SH} is the helix that is disordered in the *E. coli* structures (residues 119−128). Color coded from N (blue) to C terminus (red). (b) Stereoview of the superposition of unliganded human GAR Tfase at pH 8.5 and *E. coli* GAR Tfase (PDB code 1C2T) (grey). Human GAR Tfase is colored by its rms deviation from *E. coli* GAR Tfase with the rms deviations of less than 1 Å represented by green, rms deviations of 1 Å − 1.8 Å by yellow, and rms deviations greater than 1.8 Å by red.

rystallized crystals at pH 4.2 are structurally similar to the unliganded human GAR Tfase at the same pH (lgar) with no substrate density present in the substrate binding site. The data collection, processing, and model refinement statistics are summarized in Table 1. The human GAR Tfase residues are numbered according to *E. coli* GAR Tfase unless specified.

The human GAR Tfase model at pH 8.5 (hgar) consists of the residues 810−1007 from the trifunctional protein (purD−purM−purN) with an additional three residues (Arg, Ile, Leu) at the N-terminus resulting from expression with the pet23d vector. The C-terminal residues are flexible; the last three GAR Tfase residues and the C-terminal poly-His tag could not be traced. The human GAR Tfase protein at pH 4.2 (lgar) contains an additional two residues Ala808 and Arg809 (numbered according to the trifunctional protein sequence) because of the different truncation construct (808−1010). In this model, all of the C-terminal residues have convincing density with reasonable *B* values (average of 27 Å^2 for the last five residues of the model), as do two of the hexa-His residues. However, in the low-pH structures, the density for active site loop 141−145 is very weak, and residues 142−144 cannot be interpreted. This loop has been found to have multiple conformations in the *E. coli* GAR Tfase structures (*25*, *26*, *33*−*36*) and is generally flexible until the cofactor 10-formyl-THF or a cofactor analogue is bound.

The overall topology (Figure 2a) of human GAR Tfase, as expected, shares the same architecture as *E. coli* GAR Tfase. The structure can be divided into two subdomains that are connected through a central, mainly parallel, seven-stranded β-sheet (*34*). The N-terminal subdomain contains a Rossmann type mononucleotide fold with a phosphate ion or glycerol molecule bound to the C-terminal end of the loop connecting the first β-strand and α-helix. A long narrow cleft stretches from the phosphate-binding site to the invariant aspartic acid, Asp144, in the active site. The cleft is lined by a cluster of residues highly conserved among bacterial, yeast, avian and human enzymes (*34*). On the basis of the *E. coli* GAR Tfase complex structures, this cleft is the binding site for the cofactor and the substrate (*25*, *26*, *35*, *36*). The three independent molecules in hgar at pH 8.5 are very similar (rms deviations for the main-chain atoms of molecules A and C are 0.29 and 0.20 Å, respectively, in comparison to molecule B).

Comparison of Human and E. coli GAR Tfase Structure. *E. coli* GAR Tfase is dimeric below pH 6.75 and monomeric at higher pH (>7.5), as described from crystal structures (*25*, *26*, *33*, *36*) and biochemical studies (*18*, *37*). The dimer interface is relatively small, with a buried surface of 730

Å^2. Human GAR Tfase remains monomeric in the crystals at both pH 8.5 (hgar) and pH 4.2 (lgar). The human protein is also monomeric at pH 5 and 8 in solution, as confirmed by size exclusion chromatography (data not shown). However, the human GAR Tfase (purN) construct represents the C-terminal module of the human trifunctional protein (purD−purM−purN). The oligomeric state of human GAR Tfase in vivo will obviously be determined by the properties of the intact trifunctional enzyme. The *E. coli* purM components form a dimer, but consideration of the linker lengths that connect to purD and purN leads to a model in which two trifunctional protein molecules dimerize through purM, but the purN and purD components remain monomeric (*57*). Thus, the monomeric form of human purN in the crystal is consistent with that model.

The structure of unliganded human GAR Tfase at pH 8.5 (hgar) is highly conserved with the *E. coli* GAR Tfase despite its relatively low sequence identity (31%) (Figure 2b) (n.b. the comparison here is made with the *E. coli* GAR Tfase complex with β-GAR and 10-formyl-TDAF at pH 7.5, ref *25*, which is a high pH form and, hence, has an ordered 111−131 loop-helix). The overall rms deviation is 1.5 Å for all main-chain atoms with the major conformational changes confined to a few loops: loop 21−25, loop 58−63, the folate-dependent loop 141−146, and the N and C termini. Structure differences at the termini of the protein are not surprising, especially as they are not involved in the formyl transfer reaction and their sequence is not conserved. The conformational change for loop 21−25 likely reflects a sequence difference of Thr24 to Pro in the middle of the loop. This loop is located far from the active site, which suggests that it has no direct role in the formyl transfer reaction. However, loop 58−63 is located at the entrance of the cleft where the cofactor and substrate bind. Superposition of various *E. coli* and human GAR Tfase structures suggests that this loop may be involved in the binding of the polyglutamated tail of the folate cofactor. The different conformations of folate-bound loop 141−146 appear to be essential in the catalytic mechanism. The loop is only well ordered in complex with folate or analogues in a conformation that most likely facilitates the formyl transfer reaction (see below).

Residues 111−131. In all of the *E. coli* GAR Tfase structures, residues 111−131 are disordered (*33*−*36*), or have high *B* values which indicate relatively high flexibility. Only at a pH higher than 6.8 does the loop appear to be ordered (*25*). In the 3.0 and 2.8 Å structures of *E. coli* GAR Tfase at pH 6.75, these residues were not observed in the electron density map (*34*, *35*). In the mutant E70A structure, at pH 3.5, this loop is disordered, while at pH 7.5, it forms a loop-helix structure, but with an average *B* value of 59 Å^2, nearly double that of the overall average *B* value (31 Å^2) for the protein. It has been proposed that one of the consequences of ordering of the loop-helix is the formation of a hydrogen bond between the main-chain carbonyl of Tyr115 and the side chain of His108, which could affect both the position and pK_a of the essential active site residue His108. Also, the loop-helix formed by residues 111−131 could provide a hydrophobic lid to the active site (*33*) in the presence of the substrate. These *E. coli* structures suggested that the pH-dependent activity of *E. coli* GAR Tfase may be attributed to a disorder−order transition of the loop-helix 111−131.

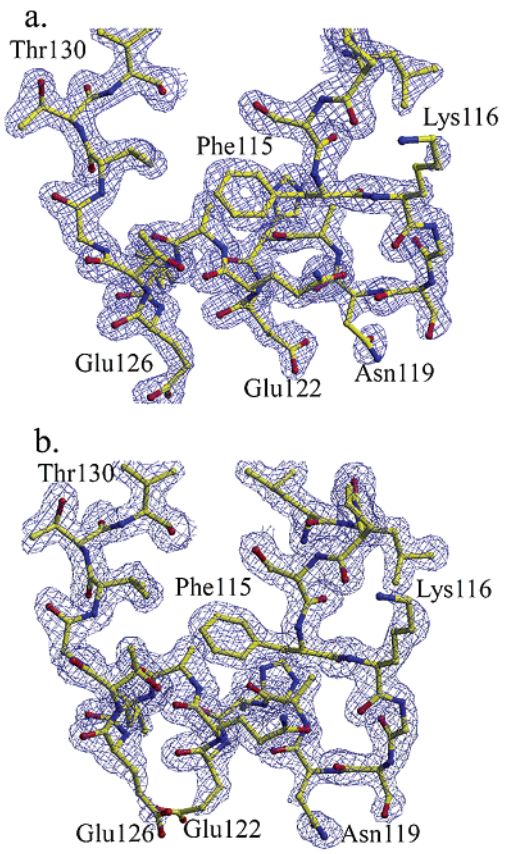

FIGURE 3: The loop-helix 111−131 conformation in human GAR Tfase. The 2Fo−Fc electron density map of the loop 111−131 of human GAR Tfase in contoured at 2σ. The refined model is superimposed on the density with the oxygen atoms colored red, nitrogen atoms blue, and bonds/carbon atoms yellow. (a) the final model and electron density map at pH 8.5 (hgar); (b) the final model and electron density map at pH 4.2 (lgar). In both structures, the loop is well ordered and forms a loop-helix structure, while in the *E. coli* enzyme, this loop is only ordered above pH 7.

Although Tyr115 is replaced by Phe in human GAR Tfase, this hydrogen bond is conserved (3.15 Å in human vs 2.6 Å in *E. coli*), since the interaction is between His108 and the main-chain carbonyl of residue 115. However, compared to the structure of the *E. coli* enzyme, residues 111−131 of human GAR Tfase are well ordered at pH 8.5 (Figure 3a) and at pH 4.2 (Figure 3b) with low *B* values (23.5 Å^2 at pH 8.5 and 27.5 Å^2 at pH 4.2). In other human GAR Tfase structures now in refinement (Zhang et al., unpublished data) in complex with different inhibitors at various pH values (4, 5.5, 6.5, 7.3, 8), none of these structures show a disordered loop-helix 111−131. Thus, the loop-helix in human GAR Tfase exhibits a similar conformation under different pH conditions. Otherwise, when compared to the *E. coli* enzyme, differences in this loop are minor, except for an rms deviation of 2 Å for residue 116, which is most likely caused by its mutation from Pro to Val. Any disorder−order transition of the loop-helix in the active site that is used to regulate the pH-dependent *E. coli* GAR Tfase activity is, therefore, not likely for the human GAR Tfase enzyme.

Comparison of Human GAR Tfase at High and Low pH. The overall rms deviation is only 1.1 Å between the human GAR Tfase at pH 8.5 (hgar) and pH 4.2 (lgar). The only significant changes are in the substrate-binding loop 8−14, the folate-dependent loop 141−145, and the flexible loop 57−63. The C-terminal residues, Lys201, Glu202, and

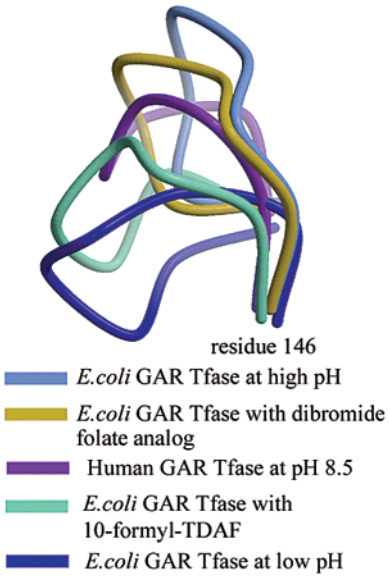

FIGURE 4: Conformational variation of the folate-dependent loop 139−146. The loop 139−146 conformation for phosphate-bound *E. coli* GAR Tfase mutant E70A at pH 7.5 (PDB code 3GAR) is colored lilac and dark-blue at pH 3.5 (PDB code 2GAR). The wild-type *E. coli* enzyme in complex with a dibromide folate analogue (PDB code 1JKX) is in khaki, and the complex structure of the folate analogue 10-formyl-TDAF (PDB code 1C2T) is colored green. In human GAR Tfase at pH 8.5, the loop is colored purple, whereas at pH 4.2 it is highly flexible and disordered.

Glu203, which are disordered at pH 8.5 (hgar), are ordered at pH 4.2 (lgar), and so are two residues of the poly-His tag. As the C-terminal and loop 57−63 residues are not thought to be directly involved in the formyl transfer reaction, we will only focus on differences in the substrate and cofactor binding sites.

Cofactor Binding Site. In the *E. coli* GAR Tfase structure, the folate-binding loop 141−145 displays different conformations under different conditions and in complex with different inhibitors (Figure 4). Without folate or a folate-analogue in the active site, the loop is very flexible (*33*, *34*). In human GAR Tfase at pH 8.5 (hgar), the loop has a *B* value of 47 Å^2 (protein average *B* value of 29.9 Å^2), and at pH 4.2, residues 142−144 in the loop are untraceable. Comparison of the human GAR Tfase with various *E. coli* GAR Tfase structure shows this loop adopts a variety of conformations (Figure 4). Residue Asp144 is essential for catalytic activity, and the conformation of this loop has important implications for inhibitor design. However, there is no evidence that the loss of activity of the protein at low pH is due to the conformational isomerism of this loop.

Substrate Binding Pocket. In all of the published *E. coli* GAR Tfase structures, the enzyme always binds to a phosphate group at its substrate-binding site, either inorganic phosphate ion from the purification/crystallization buffer or the phosphate moiety from the substrate or inhibitor (*25*, *26*, *33*−*35*). The binding of phosphate group in the *E. coli* enzyme is so tight that, even in phosphate-free purification and crystallization conditions, a phosphate group is always found at that location. Most of the interactions between the phosphate group and enzyme are among the phosphate oxygens with the backbone amide nitrogens of residues 10−13, along with a hydrogen bond to the side-chain amide of Asn13 (*34*). The conformation of this phosphate/substrate binding loop is almost identical in all of the different *E. coli* GAR Tfase structures (*25*, *26*, *33*−*36*).

The loop sequence 8−14 is conserved in human GAR Tfase with only one mutation from Asn10 to Thr, and its conformation at pH 8.5 (hgar) is similar to that of the *E. coli* enzyme. However, in two of the three NCS-related molecules (A and C), a loosely bound glycerol is found in the substrate-binding site. The glycerol likely comes from the 10% glycerol buffer used in the first step of purification.

The other molecule (molecule B) shows beautiful tetrahedral phosphate ion electron density (Figure 6a), similar to that found in *E. coli* GAR Tfase. The phosphate group is located at the very end of the active site cleft between the N and C subdomains, at the turn connecting the first β-strand and α-helix that contains the GXG motif. The helix dipole and the accessible amide hydrogens are favorable for binding negatively charged ions (reviewed in ref *58*). At pH 8.5, the prominent species for phosphate ion is HPO_4^{2-}; the phosphate oxygen O4 forms an electrostatic interaction (2.7 Å) with Lys170. The side chain of Ser12 also forms a strong hydrogen bond of 2.6 Å with the phosphate, as well as a hydrogen bond with His174 NE2 (3.3 Å). The oxygen atoms of the phosphate ion also form numerous hydrogen bonds with the backbone amides of Gly11, Ser12, and Asn13 (Figure 6d). Further interactions are formed between the

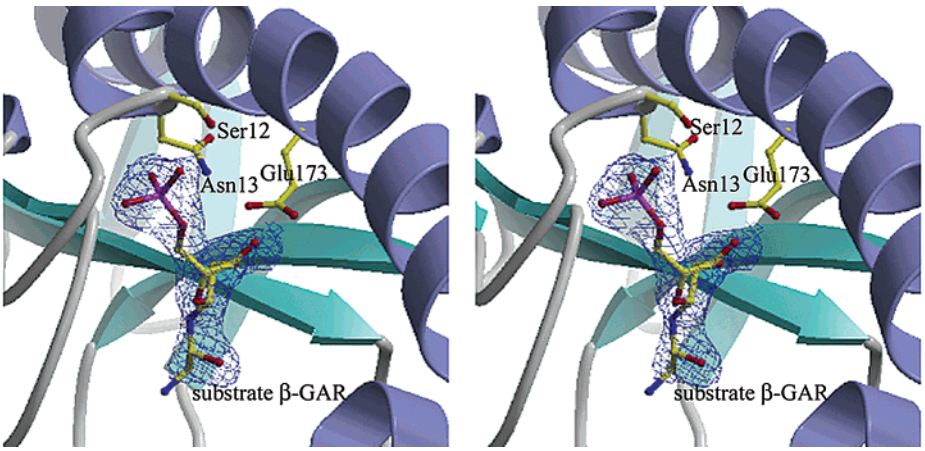

FIGURE 5: Stereoview of substrate β-GAR binding site of human GAR Tfase at pH 8.5. The enzyme is illustrated by ribbon diagram with the side chains of Ser12, Asn13, and Glu173 in ball-and-stick. The substrate, β-GAR, is represented by ball-and-stick and fitted into the 2Fo−Fc electron density map contoured at 1.4σ.

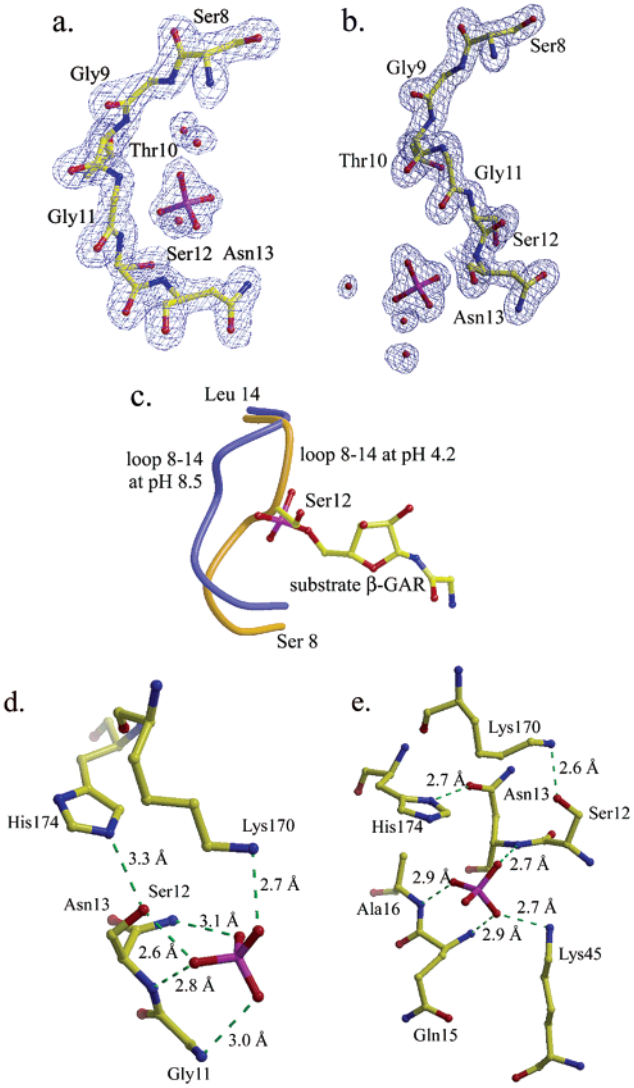

FIGURE 6: Open and occluded conformations of the substrate-binding loop 8−14. (a) Electron density and coordinates of the phosphate ion bound to the substrate-binding loop 8−14 at pH 8.5 (hgar). The density shown is from a 2Fo−Fc map contoured at 2σ. The phosphorus atom is colored magenta, oxygen red, nitrogen blue, and bonds/carbon atoms yellow. (b) Electron density and coordinates of the phosphate ion bound to the substrate-binding loop 8−14 at pH 4.2. The density shown is from a 2Fo−Fc map contoured at 2σ. Coloring of atoms is as described above. (c) Superposition of the substrate-binding loop 8−14 in unliganded enzyme at pH 4.2 onto the equivalent substrate-bound structure and enzyme at pH 8.5. Blue represents the complex structure at pH 8.5 with the substrate β-GAR in ball-and-stick. The orange loop represents the conformation at pH 4.2. (d) Interaction of phosphate ion and enzyme at pH 8.5. (e) Interaction of phosphate ion and enzyme at pH 4.2.

phosphate-oxygens and ordered solvent waters (S1, S9, S16, S117, S160, S165).

Substrate β-GAR, which incorporates a phosphate group and a ribonucleotide, was dissolved in the mother liquor at a concentration of 2 mM and the human GAR Tfase crystal was soaked in this substrate solution overnight at 4 °C at pH 8.5 (Table 1). The structural changes in the enzyme upon substrate binding are minimal. The inorganic phosphate in molecule B is replaced by the phosphoryl group from the substrate (Figure 5). The oxygen atoms OE1 and OE2 of the ribose ring of the substrate form three hydrogen bonds with Glu173 (2.5, 2.6, and 2.8 Å). The side chain of Glu173 swings toward the hydroxyls of the ribose ring to optimize hydrogen bond formation. For molecules A and C, the glycerol is replaced with β-GAR, so that these two molecules now have the same structure as molecule B. Interestingly, in the purT GAR transformylase, which also uses β-GAR as the substrate, a glutamate acid (Glu82) bridges between the 2′ and 3′ hydroxyl group of the GAR ribose as well (*59*). Yet, this is the only similarity between these two transformylases upon the binding mode of substrate β-GAR. Unlike the extensive hydrogen bonds between the phosphate group and backbone nitrogen atoms in human GAR Tfase, purT anchors the substrate by several electrostatic interactions between the phosphate moiety and side chains of positively charged residues Arg362 and Lys355 (*59*).

Unexpectedly, in the human GAR Tfase structure at pH 4.2 (lgar), the substrate-binding loop folds into the active site cleft (Figure 6b). To ensure that this significant change in the substrate binding loop residues 8−14 at different pH values is not caused by crystal packing, we analyzed the crystal lattice contacts for both the pH 8.5 and pH 4.2 models. The substrate binding loop is not involved in crystal packing in either case; therefore, the conformational change of this loop is not likely to be a crystallographic artifact, but is indicative of substrate or lack of substrate binding. Surprisingly, the phosphate position at pH 8.5 is now occupied by the side chain of Ser12 at pH 4.2 (Figure 6c). Residues 10−12 have now moved into the phosphate-binding pocket, with Gly11 and Ser12 showing rms deviations of 2.5 and 4.0 Å, respectively, compared to the human GAR Tfase structure at pH 8.5 (hgar). Concurrent with this conformational change, the phosphate ion is expelled from the pocket but, surprisingly, is still bound to the enzyme. The bound phosphate has very clear electron density and is now located in close proximity on the other face of the loop (Figure 6b). At pH 4.2, the major species of phosphate group is $H_2PO_4^-$, and the helix dipole effect is reduced in the more acidic conditions. The phosphate group has an rms deviation of 5.4 Å from its original position at pH 8.5. The negatively charged oxygen of the phosphate group favors the formation of an electrostatic interaction (2.7 Å) with Lys45. His174 is fully protonated at pH 4.2 and flips its side-chain χ2 by 180° so that its ND1 now hydrogen bonds (2.7 Å) to the side-chain oxygen of Asn13. The 4 Å shift of Ser12 now results in a strong hydrogen bond (2.6 Å) with the side-chain amide group of Lys170. The phosphate oxygen atoms still hydrogen bond with backbone amide nitrogens, but now with Asn13, Gln15, and Ala16 (Figure 6e).

To explore substrate binding at low pH, we attempted to form the substrate complex at pH 4.2. When cocrystallization was unsuccessful in revealing any substrate density, we added the substrate at a final concentration of 4 mM to preformed crystals, well above its expected K_m value (0.94 ± 0.21 μM, ref *56*). However, no density for the substrate was observed in either the cocrystallization or soaking experiments at pH 4.2, even though high-resolution structures were obtained (1.78 Å for the soaked crystal and 1.76 Å for the cocrystallized crystal). No significant differences among the three low-pH models were observed (rms deviations of 0.1 and 0.12 Å, respectively, compared to unliganded human GAR Tfase model at pH 4.2), illustrating that β-GAR does not bind at low pH.

In the human GAR Tfase at pH 8.5, the substrate binds to the enzyme by replacing the inorganic phosphate ion with

its own phosphate group. In the enzyme model at pH 4.2, an inorganic phosphate ion still binds, but now on the other face of the loop. If the substrate were to bind to the enzyme by replacing phosphate in this alternative location, the ribose ring of the substrate would sterically clash with the main chain and proximal side chains of the protein (residues 14, 15, 16, 45), or extend out of the enzyme and fail to engage in any productive hydrogen bonds between its ribose moiety and the protein.

CONCLUSIONS

Here, we present the crystal structure of human GAR Tfase, both at pH 8.5 (hgar) and at pH 4.2 (lgar). Previous studies have described inhibitors designed and targeted to the human GAR Tfase, but no structural analysis of the human enzyme has been described or coordinates deposited (*29*). Our kinetic studies revealed that the enzyme has a pH-dependent activity similar to that of *E. coli* GAR Tfase, where the protein loses activity at low pH (below 6). In our structural analysis, we showed that the substrate-binding loop (residues 8−14) has alternative conformations under different pH conditions.

Our studies with human GAR Tfase have shown that the substrate binding loop has multiple conformations with two extreme situations: open and occluded. The open conformation at pH 8.5 (hgar) binds a phosphate ion group in the active site cleft between the N and C subdomains. When the substrate is added, the phosphate moiety of the substrate displaces inorganic phosphate and forms additional favorable hydrogen bonds between the ribose ring of the substrate and the enzyme. The substrate is then positioned in the reaction cleft for nucleophilic attack on the formyl carbon of the folate cofactor.

The occluded conformation of the loop in the human GAR Tfase structure at pH 4.2 (lgar), however, shows the other extreme state, where the loop folds into the cleft and blocks phosphate binding in the substrate binding pocket. Interestingly, an alternative phosphate binding site was found adjacent to this active site loop. In this case, the substrate cannot replace the phosphate ion without clashing into the protein or sacrificing hydrogen bonds to the protein from the ribose ring. Hence, the enzyme appears to lose its activity at low pH because the substrate binding loop prohibits β-GAR substrate binding at the active site. The control of human GAR Tfase activity using occluded and open conformations of substrate binding site provides an intriguing feature for the mechanistic evaluation of the enzyme and for drug design efforts. Finally, the human GAR Tfase studies indicate that the loop-helix disorder need not be considered in mechanistic or inhibitor studies, that conformational isomerism of the active site 140−145 loop is still an issue, and that the substrate binding loop occludes the substrate binding site at low pH.

ACKNOWLEDGMENT

We thank J. Stevens for the synthesis of cloneII, X. Dai for the help of data collection and processing, N. Larsen, R. Zhu, X. Zhu, and J. Smith for valuable suggestions, M. Elsliger for computational assistance, and the staff of SSRL beamline 9-1 and 11-1 and ALS beamline 5.0.2 for technical support in X-ray data collection.

REFERENCES

1. Dev, I. K., and Harvey, R. J. (1978) *J. Biol. Chem. 253*, 4242−4244.
2. Caperelli, C. A. (1989) *J. Biol. Chem. 264*, 5053−5057.
3. Inglese, J., Johnson, D. L., Shiau, A., Smith, J. M., and Benkovic, S. J. (1990) *Biochemistry 29*, 1436−1443.
4. Davies, J. F. D., Delcamp, T. J., Prendergast, N. J., Ashford, V. A., Freisheim, J. H., and Kraut, J. (1990) *Biochemistry 29*, 9467−9479.
5. Oefner, C., D'Arcy, A., and Winkler, F. K. (1988) *Eur. J. Biochem. 174*, 377−385.
6. Montfort, W. R., Perry, K. M., Fauman, E. B., Finer-Moore, J. S., Maley, G. F., Hardy, L., Maley, F., and Stroud, R. M. (1990) *Biochemistry 29*, 6964−6977.
7. Hardy, L. W., Finer-Moore, J. S., Montfort, W. R., Jones, M. O., Santi, D. V., and Stroud, R. M. (1987) *Science 235*, 448−455.
8. Newell, D. R. (1999) *Semin. Oncol. 26*, 74−81.
9. Takimoto, C. H. (1997) *Semin. Oncol. 24*, S18−40−S18−51.
10. Taylor, E. C., Harrington, P. J., Fletcher, S. R., Beardsley, G. P., and Moran, R. G. (1985) *J. Med. Chem. 28*, 914−921.
11. Beardsley, G. P., Moroson, B. A., Taylor, E. C., and Moran, R. G. (1989) *J. Biol. Chem. 264*, 328−333.
12. Moran, R. G. (1983) *Adv. Exp. Med. Biol. 163*, 327−339.
13. Shane, B., Bognar, A. L., Goldfarb, R. D., and LeBowitz, J. H. (1983) *J. Bacteriol. 153*, 316−325.
14. McGuire, J. J., Hsieh, P., and Bertino, J. R. (1984) *Biochem. Pharmacol. 33*, 1355−1361.
15. Baldwin, S. W., Tse, A., Gossett, L. S., Taylor, E. C., Rosowsky, A., Shih, C., and Moran, R. G. (1991) *Biochemistry 30*, 1997−2006.
16. Moran, R. G., and Colman, P. D. (1984) *Biochemistry 23*, 4580−4589.
17. Chabner, B. A., Allegra, C. J., Curt, G. A., Clendeninn, N. J., Baram, J., Koizumi, S., Drake, J. C., and Jolivet, J. (1985) *J. Clin. Invest. 76*, 907−912.
18. Mullen, C. A., and Jennings, P. A. (1996) *J. Mol. Biol. 262*, 746−755.
19. Schild, D., Brake, A. J., Kiefer, M. C., Young, D., and Barr, P. J. (1990) *Proc. Natl. Acad. Sci. U.S.A. 87*, 2916−2920.
20. Daubner, S. C., Young, M., Sammons, R. D., Courtney, L. F., and Benkovic, S. J. (1986) *Biochemistry 25*, 2951−2957.
21. Aimi, J., Qiu, H., Williams, J., Zalkin, H., and Dixon, J. E. (1990) *Nucleic Acids Res. 18*, 6665−6672.
22. Warren, M. S., Marolewski, A. E., and Benkovic, S. J. (1996) *Biochemistry 35*, 8855−8862.
23. Inglese, J., Smith, J. M., and Benkovic, S. J. (1990) *Biochemistry 29*, 6678−6687.
24. Shim, J. H., and Benkovic, S. J. (1998) *Biochemistry 37*, 8776−8782.
25. Greasley, S. E., Yamashita, M. M., Cai, H., Benkovic, S. J., Boger, D. L., and Wilson, I. A. (1999) *Biochemistry 38*, 16783−16793.
26. Greasley, S. E., Marsilje, T. H., Yamashita, M. M., Cai, H., Benkovic, S. J., Boger, D. L., and Wilson, I. A. (2001) *Biochemistry 40*, 13538−13547.
27. Boger, D. L., Marsilje, T. H., Castro, R. A., Hedrick, M. P., Jin, Q., Baker, S. J., Shim, J. H., and Benkovic, S. J. (2000) *Bioorg. Med. Chem. Lett. 10*, 1471−1475.
28. Marsilje, T. H., Labroli, M. A., Hedrick, M. P., Jin, Q., Desharnais, J., Baker, S. J., Gooljarsingh, L. T., Ramcharan, J., Tavassoli, A., Zhang, Y., Wilson, I. A., Beardsley, G. P., Benkovic, S. J., and Boger, D. L. (2002) *Bioorg. Med. Chem. 10*, 2739−2749.
29. Varney, M. D., Palmer, C. L., Romines, W. H., 3rd, Boritzki, T., Margosiak, S. A., Almassy, R., Janson, C. A., Bartlett, C., Howland, E. J., and Ferre, R. (1997) *J. Med. Chem. 40*, 2502−2524.
30. Ferone, R., Singer, S. C., and Hunt, D. F. (1986) *J. Biol. Chem. 261*, 16363−16371.
31. Ferone, R., Hanlon, M. H., Singer, S. C., and Hunt, D. F. (1986) *J. Biol. Chem. 261*, 16356−16362.
32. Shim, J. H., and Benkovic, S. J. (1999) *Biochemistry 38*, 10024−10031.
33. Su, Y., Yamashita, M. M., Greasley, S. E., Mullen, C. A., Jennings, P. A., Warren, M. S., Benkovic, S. J., and Wilson, I. A. (1998) *J. Mol. Biol. 281*, 485−499.
34. Chen, P., Schulze-Gahmen, U., Stura, E. A., Inglese, J., Johnson, D. L., Marolewski, A., Benkovic, S. J., and Wilson, I. A. (1992) *J. Mol. Biol. 227*, 283−292.

35. Almassy, R. J., Janson, C. A., Kan, C. C., and Hostomska, Z. (1992) *Proc. Natl. Acad. Sci. U.S.A. 89*, 6114−6118.
36. Klein, C., Chen, P., Arevalo, J. H., Stura, E. A., Marolewski, A., Warren, M. S., Benkovic, S. J., and Wilson, I. A. (1995) *J. Mol. Biol. 249*, 153−175.
37. Mullen, C. A., and Jennings, P. A. (1998) *J. Mol. Biol. 276*, 819−827.
38. Rayl, E. A., Moroson, B. A., and Beardsley, G. P. (1996) *J. Biol. Chem. 271*, 2225−2233.
39. Boschelli, D. H., Webber, S., Whiteley, J. M., Oronsky, A. L., and Kerwar, S. S. (1988) *Arch. Biochem. Biophys. 265*, 43−49.
40. Caperelli, C. A., and Giroux, E. L. (1997) *Arch. Biochem. Biophys. 341*, 98−103.
41. Fulop, V., Szeltner, Z., Renner, V., and Polgar, L. (2001) *J. Biol. Chem. 276*, 1262−1266.
42. Ducruix, A., and Giege, R. (1992) *Crystallization of Nucleic Acids and Proteins: A Practical Approach*, Oxford University Press, New York.
43. Otwinowski, Z., and Minor, W. (1997) *Methods Enzymol. 276*, 307−326.
44. Matthews, B. W. (1968) *J. Mol. Biol. 33*, 491−497.
45. Rossmann, M. G. (1972) *The Molecular Replacement Method*, Gordon & Breach, New York.
46. CCP4. (1994) *Acta Crystallogr. D50*, 760−763.
47. Navaza, J. (1994) *Acta Crystallogr. A50*, 157−163.
48. Marangos, P. J., Loftus, T., Wiesner, J., Lowe, T., Rossi, E., Browne, C. E., and Gruber, H. E. (1990) *Epilepsia 31*, 239−246.
49. Brünger, A. T., Krukowski, A., and Erickson, J. W. (1990) *Acta Crystallogr. A46*, 585−593.
50. Jones, T. A., Zou, J. Y., Cowan, S. W., and Kjeldgaard, M. (1991) *Acta Crystallogr. A47*, 110−119.
51. Jiang, J. S., and Brünger, A. T. (1994) *J. Mol. Biol. 243*, 100−115.
52. Cowtan, K. D., and Main, P. (1996) *Acta Crystallogr. D52*, 43−48.
53. Winn, M. D., Isupov, M. N., and Murshudov, G. N. (2001) *Acta Crystallogr. D57*, 122−133.
54. Laskowski, R. A., MacArthur, M. W., Moss, D. S., and Thornton, J. M. (1993) *J. Appl. Crystallogr. 26*, 283−291.
55. Kan, C. C., Gehring, M. R., Nodes, B. R., Janson, C. A., Almassy, R. J., and Hostomska, Z. (1992) *J. Protein Chem. 11*, 467−473.
56. Poch, M. T., Qin, W., and Caperelli, C. A. (1998) *Protein Expr. Purif. 12*, 17−24.
57. Li, C., Kappock, T. J., Stubbe, J., Weaver, T. M., and Ealick, S. E. (1999) *Structure Fold Des. 7*, 1155−1166.
58. Hol, W. G. (1985) *Adv. Biophys. 19*, 133−165.
59. Thoden, J. B., Firestine, S., Nixon, A., Benkovic, S. J., and Holden, H. M. (2000) *Biochemistry 39*, 8791−8802.

BI020522M